Eur. Phys. J. B **17**, 449–457 (2000)

THE EUROPEAN PHYSICAL JOURNAL B

EDP Sciences

Two-variable macroscopic model for spin-crossover solids: Static and dynamic effects of the correlations

B. Hôo[a], K. Boukheddaden, and F. Varret

Laboratoire de Magnétisme et d'Optique, Université de Versailles[b], 45 avenue des États-Unis, 78035 Versailles Cedex, France

Received 20 April 2000

Abstract. In order to investigate the role of nearest neighbors correlations in the relaxation of the High Spin fraction in spin crossover compounds, we have developed a two macro-variable dynamical model based on Kubo's treatement of the master equation. This is compared to the local equilibrium approach, where short-range correlations are assumed to follow adiabatically the long range-order parameter. The sigmoidal shape of the relaxation, previously associated with the effects of interactions, and the so-called "tail effect", *i.e.* the extra-slowing down at long times due to the correlations are obtained. The accurate comparison to experimental relaxation data confirms the coexistence of short-range and long-range interactions in spin-crossover solids.

PACS. 64.60.-i General studies of phase transition – 05.70.Ln Nonequilibrium and irreversible thermodynamics – 05.50.+q Lattice theory and statistics (Ising, Potts, etc.)

1 Introduction

Spin crossover compounds, which have been studied for a number of years [1], are examples of molecular bistable solids. Their bistability, originating from intra-molecular vibronic coupling, can be enhanced by inter-molecular interactions, which are elastic in nature, and these may induce a 1st order transition with thermal hysteresis loop. The width of the loop depends on the strength of the coupling. Due to their bistable character, these systems are potential candidates for information storage applications. In the 1980's, the Mainz group [2] discovered that, under optical irradiation with a selected wavelength (550 nm), at low temperature, these compounds could be converted from Low Spin (LS) to High Spin (HS) state. The phenomenon was called LIESST (Light Induced Excited Spin State Trapping) and the HS state is populated via intermediate, high-energy, vibronic states which rapidly decay according to non-adiabatic, non-radiative processes. The LIESST effect, which later was shown to be reversible, has lead to a large number of investigations of the metastable, photo-excited states, namely the post-LIESST relaxation in pure and diluted compounds. All data show that the relaxation curves (population of the excited state *vs.* time) of cooperative systems have a typical sigmoidal shape, associated with a "self-accelerated" relaxation [3]. Such curves have been successfully reproduced, when the cooperativity was not too strong, by a phenomenological formula closely related to the available mean-field models. A recent analytical calculation has thrown some light on the microscopic origin of this phenomenological formula [4]. This was a dynamic extention of a previous static microscopic Ising-like model introduced for the spin transitions by Wajnflasz and Pick [5] later revisited for example for the binuclear or the two-sublattice systems [6,7]. Independently, Doniach *et al.* [8], used the Ising-like model for phospholipid bilayers, showed the equivalence with the simple Ising model, under a temperature-dependant field which substitutes the effect of the different degeneracies of the two levels. However, experimental relaxation curves of highly cooperative systems show an extra slowing down of the relaxation at long times, which is not explained by the mean-field approach, the so-called tailed effect, but could be reproduced by the Monte-Carlo simulations, carried out by Romstedt *et al.* [9], and therefore could be assigned to the development of correlations due to the presence of short-range interactions.

The present work also focuses on the role of correlations, and provides an analytical approach of the problem. We treat the master equation in terms of macrovariables, following the method introduced by Kubo *et al.* [10]. The mean field approximation of the master equation due to Suzuki and Kubo [11] is extended here to spin crossover problem, taking effect of first-neighbour correlations into account, leading to the dynamics associated with the Bethe Peierls approximation [12]. The analytical resolution can advantageously substitute for the Monte-Carlo simulations which require extremely long computer times when the low temperature processes are to be investigated. In addition, the present analytical model could

[a] e-mail: hoo@physique.uvsq.fr
[b] UMR 8634 du CNRS

be suited to further developments, *e.g.* the extension to diluted systems.

2 The Hamiltonian and the evolution equation

2.1 The Ising-like Hamiltonian

In the Ising-like Hamiltonian proposed by Wajnflasz and Pick, the two levels have different degeneracies. We denote g_-, g_+ the degeneracies of the LS, HS states respectively, $g = \frac{g_+}{g_-} > 1$ is the degeneracy ratio, $\Delta > 0$ the ligand field (such that the LS state is the ground state), and J the interaction between the molecules, assumed to have an independant value on spin state. Accounting for the isomorphism [8] between the Ising-like model and an Ising model under a temperature dependant field, the Hamiltonian is written:

$$H = -J \sum_{\langle i,j \rangle} \sigma_i \sigma_j - \left(\frac{kT}{2} \ln \left(\frac{g_+}{g_-} \right) - \Delta \right) \sum_i \sigma_i \quad (2.1)$$

where $\sum_{\langle i,j \rangle}$ is the sum over the interacting neighbours.

The mean-field resolution of this Hamiltonian has been widely presented, in static and, recently, dynamic models [4]. We now include the effect of the first-neighbour correlations, *i.e.* we follow the Bethe Peierls approximation.

Let us consider a lattice of N spins. N_+, N_- respectively denote the number of HS, LS molecules. Their difference X represents the "magnetization" of the system:

$$N_+ + N_- = N \quad (2.2)$$
$$N_+ - N_- = X. \quad (2.3)$$

The pairs of neighbours are denoted accordingly: N_{++}, N_{+-}, N_{-+}, N_{--}, and obey the following constraints:

$$N_{++} + N_{--} + Q = \frac{zN}{2} \quad (2.4)$$
$$N_{++} + \frac{Q}{2} = \frac{zN_+}{2} \quad (2.5)$$
$$N_{--} + \frac{Q}{2} = \frac{zN_-}{2} \quad (2.6)$$

with z the coordination (number of first neighbours of a given molecule) and $Q = N_{+-} + N_{-+}$ the number of pairs in the mixed states HS-LS and LS-HS. The energy of the system is expressed in terms of the two macro-variables X, Q:

$$E(X,Q) = -\frac{zN}{2} J + 2JQ - \left(\frac{kT}{2} \ln(g) - \Delta \right) X. \quad (2.7)$$

For convenience, we introduce intensive macro-variables x, q associated with X, Q:

$$x = \frac{X}{N} \qquad q = \frac{Q}{N} \cdot \quad (2.8)$$

The usual notations for the spin-crossover community are: n_{H} relative population of the HS state, n_{HL} relative population of the *mixed* states (HS-LS and LS-HS) of the pairs. These are straightforwardly related to the above macro-variables:

$$n_{\mathrm{H}} = \frac{N_+}{N} = \frac{N+X}{2N} = \frac{1+x}{2} \quad (2.9)$$
$$n_{\mathrm{HL}} = \frac{Q}{\frac{zN}{2}} = \frac{N_{+-} + N_{-+}}{\frac{zN}{2}} = \frac{2q}{z} \cdot \quad (2.10)$$

The equilibrium properties of the model can be derived from equations (2.1–2.6), leading to the self-consistent equation of the static Bethe Peierls model. In the present report, we rather start with the dynamical treatement of the model, and afterwards derive the static properties, which are already known and thus provide a relevance check of the treatment.

2.2 The evolution equation

We follow here the van Kampen development [13] of the master equation. For this, considering markovian dynamics, we use the Chapman-Kolmogorov equation (known as the master equation too) in the discrete case. The latter is written in the one-variable case:

$$\frac{\partial P(a;t)}{\partial t} = \sum_{a'} W(a \mid a') P(a';t) - \sum_{a'} W(a' \mid a) P(a;t) \quad (2.11)$$

where $P(a;t)$ is the probability density for the system to be in configuration a at time t, and $W(a \mid a')$ the rate transition for the system to move from configuration a' to configuration a.

In the present two macro-variables (X, Q) case, we express the transition rate as a function of both the initial state (X, Q) and the length of the jump $(\delta X, \delta Q)$.

$$W(a \mid a') = W(X, Q \mid \delta X, \delta Q). \quad (2.12)$$

For convenience, and also for the coherence in the choice of the intensive macro-variables, the transition rate is re-expressed:

$$w(x, q, \delta X, \delta Q) = N^{-1} W(X, Q \mid \delta X, \delta Q). \quad (2.13)$$

The van Kampen development yields the following set of evolution equations (for the detailed derivation, see [14]).

$$\frac{\mathrm{d}\overline{x}(t)}{\mathrm{d}t} = \sum_{\delta X} \sum_{\delta Q} \delta X w(x, q, \delta X, \delta Q) \quad (2.14)$$
$$\frac{\mathrm{d}\overline{q}(t)}{\mathrm{d}t} = \sum_{\delta X} \sum_{\delta Q} \delta Q w(x, q, \delta X, \delta Q). \quad (2.15)$$

3 The dynamic choice

To choose the transition rates, we follow Kubo and Saito [10] who treat a cluster made of a central atom and its first neighbours as representative of the system. Their approximation realises a cut-off of the inter-cluster interactions, analogous to the static Bethe-Peierls treatment [12]. For simplicity we use the "magnetic" notations associated with the (fictitious) spins of the Ising Hamiltonians.

The central spin can be flipped by thermal fluctuations, and we start with the case of a central spin in the "up" (+) state. It is surrounded by k up spins and $z-k$ down spins. When the central spin flips, the magnetisation of the system increases by $\delta X = -2$ and the number of mixed pairs by $\delta Q = 2k - z$. The transition rate is assumed to be the product of the flipping probability by the number of suited configurations of the system, Ω, expressed as [10,15]:

$$\begin{aligned}\Omega &\simeq N_+ \frac{C^k_{N_{++}} C^{z-k}_{N_{+-}}}{C^z_{\frac{z}{2}N_+}} \\ &\simeq N_+ C^k_z \frac{N^k_{++}\left(\frac{Q}{2}\right)^{z-k}}{\left(\frac{zN_+}{2}\right)^z}\end{aligned} \tag{3.1}$$

which is the average number of up spins multiplied by the number of different ways for taking k pairs (++) out of N_{++}, multiplied by the number of different ways for taking $z-k$ pairs (+−) out of N_{+-}, and divided by the number of equivalent permutations. To derive the second expression we applied the Tagaki approximation [15].

The microscopic transition rates $w_{\rm m}(\sigma_0, k)$ of the central spin in the initial states σ_0 also obey the detailed balance equation:

$$\begin{aligned}w_{\rm m}(\sigma_0 = +1, k) P_{\rm e}(\sigma_0 = +1, k) = \\ w_{\rm m}(\sigma_0 = -1, k) P_{\rm e}(\sigma_0 = -1, k)\end{aligned} \tag{3.2}$$

with $P_{\rm e}(\sigma_0, k)$ the corresponding equilibrium probabilities of the cluster. This leads to:

$$\frac{w_{\rm m}(\sigma_0 = +1, k)}{w_{\rm m}(\sigma_0 = -1, k)} = {\rm e}^{-\beta \Delta E} \tag{3.3}$$

with $\Delta E = E(X-2, Q+2k-z) - E(X, Q)$ the energy difference between the final and the initial states of the cluster.

Since equation (3.3) does not separately provide the up and down transition rates (but only their ratio), a dynamic choice has to be made. This is quite general for the dynamic approaches based on a time-independent Hamiltonian. Following Kubo and Saito [10], we make the following choice:

$$w_{\rm m}(\sigma_0 = +1, k) = \frac{1}{\tau} {\rm e}^{-\beta \frac{\Delta E}{2}} \tag{3.4}$$

$$w_{\rm m}(\sigma_0 = -1, k) = \frac{1}{\tau} {\rm e}^{\beta \frac{\Delta E}{2}}. \tag{3.5}$$

More precisely, for a spin up (+) surrounded by k spins up, the transition rate writes:

$$w_{\rm m}(\sigma_0 = +1, k) = \frac{1}{\tau} {\rm e}^{K(z-2k)+\mu} \tag{3.6}$$

with $K = J/kT$ and $\mu = \left(\frac{kT}{2}\ln(g) - \Delta\right)/kT$.

A Glauber-type dynamic choice [16] would lead to:

$$w^{\rm G}_{\rm m}(\sigma_0 = +1, k) = \frac{1}{2\tau}\left(1 - \sigma_0 \tanh\left(\beta \Delta E\right)\right). \tag{3.7}$$

Experimental data for spin crossover compounds established the presence of an intramolecular energy barrier [1,3]. The role of interactions on the intramolecular barrier energy $E_{\rm a}$, was first described with a phenomenological macroscopic model [3], and later supported by a microscopic cooperative dynamic model [4]. The presence of the energy barrier is accounted for here (as in [4]) through the Arrhenius-type expression of the individual flipping frequency:

$$\frac{1}{\tau} = \frac{1}{\tau_0} {\rm e}^{-\beta E_{\rm a}}. \tag{3.8}$$

The barrier energy in equation (3.8) here does not account for the effect of interactions, since these are already involved in the previous expressions of the transition rates (through the energy values). It is worth noting that the Kubo and Saito choice merely adds the intramolecular barrier energy and the interaction energies. Finally, the flipping rates are expressed as:

$$\begin{aligned}W_+(X, Q \to X-2, Q+2k-z) = \\ \frac{1}{\tau_0} {\rm e}^{-\beta E_{\rm a}} \Omega {\rm e}^{K(z-2k)+\mu} \\ = \frac{1}{\tau_0} {\rm e}^{-\beta E_{\rm a}} N_+ C^k_z \frac{N^k_{++}\left(\frac{Q}{2}\right)^{z-k}}{\left(\frac{zN_+}{2}\right)^z} {\rm e}^{K(z-2k)+\mu}.\end{aligned} \tag{3.9}$$

They are re-expressed in terms of x, q:

$$\begin{aligned}w_+(x, q, \delta X = -2, \delta Q = 2k - z) = \\ N^{-1} W_+(X, Q \to X-2, Q+2k-z) \\ = \frac{1}{\tau_0} {\rm e}^{-\beta E_{\rm a}} \frac{1+x}{2} C^k_z \frac{\left(\frac{\frac{z}{2}(1+x)-q}{2}\right)^k \left(\frac{q}{2}\right)^{z-k}}{\left(\frac{z\left(\frac{1+x}{2}\right)}{2}\right)^z} {\rm e}^{K(z-2k)-\mu}\end{aligned} \tag{3.10}$$

The case of the central spin in the "down" (-) state straightforwardly follows, by just interchanging up and down everywhere in the previous developments. We obtain:

$$\begin{aligned}w_-(x, q, \delta X = 2, \delta Q = 2k - z) = \\ N^{-1} W_-(X, Q \to X+2, Q+2k-z) \\ = \frac{1}{\tau_0} {\rm e}^{-\beta E_{\rm a}} \frac{1-x}{2} C^k_z \frac{\left(\frac{\frac{z}{2}(1-x)-q}{2}\right)^k \left(\frac{q}{2}\right)^{z-k}}{\left(\frac{z\left(\frac{1-x}{2}\right)}{2}\right)^z} {\rm e}^{K(z-2k)-\mu}.\end{aligned} \tag{3.11}$$

The evolution equations of the macro-variables can be expressed now, using the expressions (3.10, 3.11) of $w_+(x,q,\delta X,\delta Q)$, $w_-(x,q,\delta X,\delta Q)$, where x and q are now time dependent averaged quantities (*i.e.* we have to replace x and q by $\overline{x}$ and $\overline{q}$), as:

$$\frac{\mathrm{d}\overline{x}(t)}{\mathrm{d}t} = \frac{2}{\tau_0}\mathrm{e}^{-\beta E_\mathrm{a}}\left(C_- - C_+\right) \tag{3.12}$$

$$\frac{\mathrm{d}\overline{q}(t)}{\mathrm{d}t} = \frac{z}{\tau_0}\mathrm{e}^{-\beta E_\mathrm{a}}\left(A_+C_+ + A_-C_-\right) \tag{3.13}$$

with:

$$A_\pm = \frac{\frac{\frac{z}{2}(1\pm\overline{x})-\overline{q}}{2}\,\mathrm{e}^{-K} - \frac{1}{2}\overline{q}\mathrm{e}^{K}}{\frac{\frac{z}{2}(1\pm\overline{x})-\overline{q}}{2}\,\mathrm{e}^{-K} + \frac{1}{2}\overline{q}\mathrm{e}^{K}} \tag{3.14}$$

$$\begin{aligned} C_\pm &= \sum_{k=1}^{z} w_\pm\left(\overline{x},\overline{q},\delta X,\delta Q\right) \\ &= \frac{1\pm\overline{x}}{2}\left(\mathrm{e}^{-K} + \frac{4\overline{q}\sinh\left(K\right)}{z\left(1\pm\overline{x}\right)}\right)^{z}\mathrm{e}^{\mp\mu}. \end{aligned} \tag{3.15}$$

The set of differential equations (3.12, 3.13), can be solved numerically, *e.g.* using the modified midpoint routine [17]. It provides the time evolutions of the macro-variables $\overline{x}(t)$, $\overline{q}(t)$. The static properties of the system also are obviously derived.

It can be remarked that the present equations hold for 1D systems, as well, and can easily be extended to include both long-range and short-range interactions (for spin-crossover solids, long-range are "ferro", while short-range may be "ferro" or "anti-ferro"[18]).

4 Static aspects

The static properties of the system are derived from equations (3.12, 3.13), by setting the time derivative to zero:

$$q^2 = \mathrm{e}^{-4K}\left(\frac{z}{2}\left(1+x\right)-q\right)\left(\frac{z}{2}\left(1-x\right)-q\right) \tag{4.1}$$

$$\left(\frac{1-x}{1+x}\right)^{z-1} = \mathrm{e}^{2\mu}\left(\frac{\frac{z}{2}\left(1-x\right)\mathrm{e}^{-K}+q\sinh\left(K\right)}{\frac{z}{2}\left(1+x\right)\mathrm{e}^{-K}+q\sinh\left(K\right)}\right)^{\frac{z}{2}} \tag{4.2}$$

where, for convenience, the observables $\overline{x}(t),\overline{q}(t)$ have been denoted x,q. This notation will be kept in the following. The effective field μ has been defined below equation (3.6). We recognize here the Fowler and Guggenheim equations [19], known for the so-called quasi-chemical approximation, which is strictly equivalent to the Bethe approximation [12]. Solving these equations, we could plot the temperature dependence of the HS fraction n_H at equilibrium, Figure 1. The first-order transition may occur only around the equilibrium temperature, T_eq, *i.e.* the temperature at which the effective field, μ, vanishes [8]. It is obtained only if T_eq is lower than T_OD, ordering temperature of the "pure" Ising system (without field). The idea is that the reversal of μ will induce a jump in the equilibrium magnetization, only if the "pure" system is ordered. T_eq is given by:

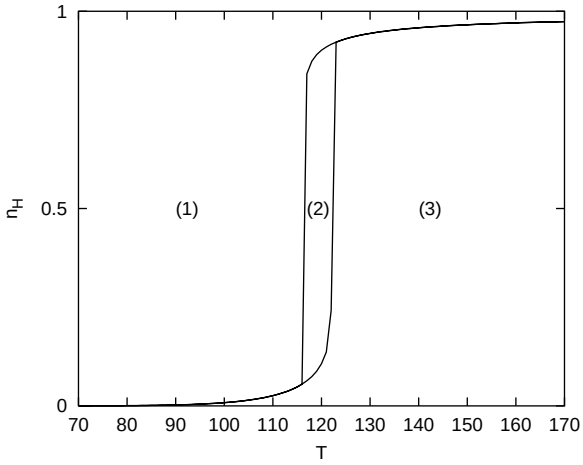

Fig. 1. Thermal hysteresis loop (the relative population of the High Spin state n_H *vs.* temperature T) computed with the present model (Bethe approximation), with: $\Delta = 300$ K, $g = 150$, $z = 4$, $J = 50$ K, leading to $T_\mathrm{equil} = 119.7$ K, $J_\mathrm{C} = 41.5$ K, which fulfill the occurrence condition for the first-order transition $J > J_\mathrm{c}$.

$$T_\mathrm{eq} = \frac{2\Delta}{k\ln\left(g\right)}\,. \tag{4.3}$$

On the other hand, in the Bethe approximation, T_OD is given by:

$$T_\mathrm{OD} = \frac{2J}{k\ln\left(\frac{z}{z-2}\right)}\,. \tag{4.4}$$

Therefore the occurrence condition of the first-order transition writes:

$$\frac{\Delta}{\ln\left(g\right)} < \frac{J}{\ln\left(\frac{z}{z-2}\right)}\,. \tag{4.5}$$

The above relation results in an interaction threshold, J_c, below which the thermal dependence of n_H is continuous, and usually denoted "spin conversion".

$$J > J_\mathrm{c} = \frac{\Delta\ln\left(\frac{z}{z-2}\right)}{\ln\left(g\right)}\,. \tag{4.6}$$

This formula can be tested for two simple particular cases: (i) it is known that short-range interactions do not order the 1D Ising system ($z = 2$); (ii) it is also known that, for z tending to infinity, the mean-field result is obtained, *i.e.* the first order criterium obtained by Wajnflasz and Pick [5] is obtained:

$$zJ > \frac{2\Delta}{\ln\left(g\right)}\,. \tag{4.7}$$

A simple extension is obtained in the model of uniform dilution, zp substituting for z, with p the relative amount of

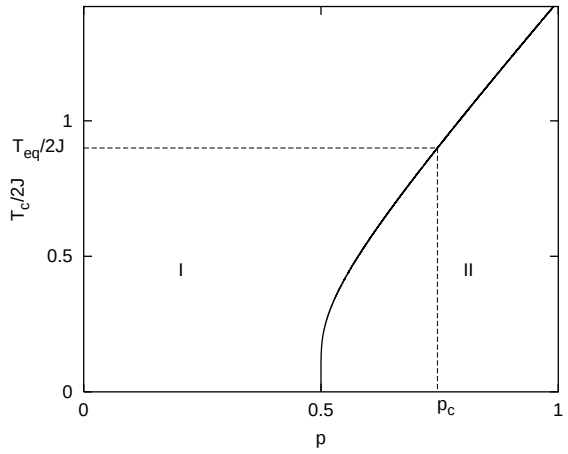

Fig. 2. Phase diagram of the diluted "pure" Ising model (no field, no degeneracies in the spin states), in reduced coordinates: $T/2J$ *vs.* p, the relative concentration of magnetic atoms, for the 2D lattice ($z = 4$). The full line is a second-order line $T_{\rm C}/2J = f(p)$ separating the ordered (domain II) and disordered states (domain I); it starts on the concentration axis at the geometric percolation threshold $p_{\rm c}^{\rm g} = 2/z$. The actual percolation threshold, $p_{\rm c}$, of the Ising-like system is given by the intersection with the horizontal dotted line of ordinate $T_{\rm equil}/2J$. The occurrence condition of the first order transition for the Ising-like system is given by the location of the "representative point" $(p, T_{\rm equil}/2J)$ in domain II.

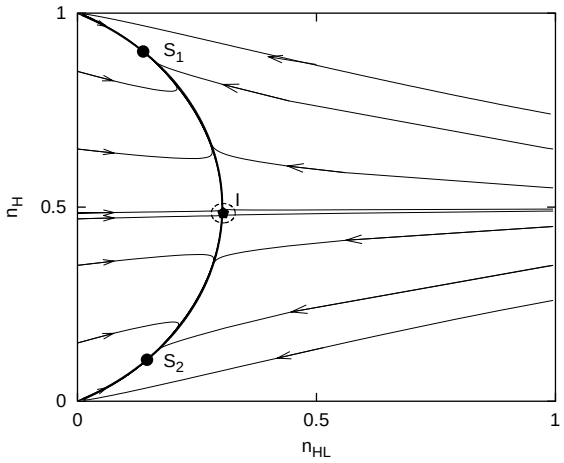

Fig. 3. Flow diagram for the kinetic Ising-like system, in the 2-macrovariable phase space, for parameter values corresponding to the static hysteresis interval: $\Delta = 300$ K, $g = 150$, $z = 4$, $J = 50$ K, (as in Fig. 1), $T = 120$ K. The timescale is not needed (for simplicity $E_{\rm a} = 0$. $\tau_0 = 1$). S_1, S_2 are the attractors of the system, I is the saddle point that all trajectories avoid, thus evidencing the bistable properties of the dynamic system. The bold curve (parabola shape), is that of the local equilibrium approximation. A remarkable feature is that all trajectories rapidly join the local equilibrium curve (bold line). Relaxation occurs in two successive (fast, adiabatic) regimes.

"spin-crossover-active" molecules in the system. A critical concentration $p_{\rm c}$ for the system to undergo the first order transition is thus derived. At $p_{\rm c}$, $T_{\rm OD} = T_{\rm eq}$, so that:

$$p_{\rm c} = \frac{2}{z} \frac{g^{\frac{J}{\Delta}}}{g^{\frac{J}{\Delta}} - 1} \cdot \tag{4.8}$$

The above equation easily shows that the actual (*i.e.* for the spin-crossover transition) critical concentration $p_{\rm c}$ is always larger than the geometrical percolation threshold $2/z$ (*i.e.* 0 in the mean-field case).

The curve $T_{\rm C}(p)$, for the true Ising system (diluted), has been plotted in Figure 2. It can be used as a phase diagram and provides the criterion for the occurrence of the first-order transition in the Ising-like diluted system (see caption of Fig. 2).

It is interesting to compare these theoretical results to the experimental data for the phase diagram of a diluted system. In the solid state, $[{\rm Fe}_p{\rm Ni}_{1-p}\,({\rm btr})_2\,({\rm NCS})_2] \cdot {\rm H_2O}$ consists of planar layers of six coordinated metals ions linked to each other in the equatorial plane. Basically, this gives the system a 2D character, which leads to take $z = 4$. Experimental data determined a percolation threshold value $p_{\rm c} = 0.44$ [20]. The present calculations (from Eq. (4.8)) lead to $p_{\rm c} = 0.65$, by taking $z = 4$, and J, Δ and g derived from the fit of experimental hysteresis loops. This disagreement might be a signature of the presence of long range interactions. Indeed, in the long range Ising model, there is no percolation effect (*i.e.* $p_{\rm c} = 0$). So, introducing long range interaction into the present model, will certainly lower the percolation threshold value. The analysis of the static data in such terms will certainly provide precious complements to the investigation of the relaxation curves, which is reported in the following.

5 Flow diagrams

The kinetic behaviour of the system out of equilibrium is conveniently described using flow diagrams, made of the trajectories of the system (for all possible initial states) in the phase space defined by the macro-variables x, q. Equations (3.12, 3.13) are easily combined in order to eliminate the time variable:

$$\frac{{\rm d}x}{{\rm d}q} = \frac{2}{z} \frac{C_- - C_+}{A_+C_+ + A_-C_-} \cdot \tag{5.1}$$

Equation (5.1) is resolved numerically (stepwise) for a large variety of initial states. The computed flow diagrams are shown for 3 different temperatures, differently located with respect to the equilibrium hysteresis loop reported in Figure 1: for the intermediate temperature value (belonging to the hysteresis interval), Figure 3, the system is bistable, *i.e.* it possesses two stable attractors (S_1 et S_2) and one unstable (I), which are obviously associated with the equilibrium states of the static hysteresis loop. For the other two temperatures, the system is monostable, *i.e.* the flow diagrams, Figures 4 and 5 have a single attractor and no singularity. We now discuss the bistable case, Figure 3, in more details. An obvious feature, almost common to all trajectories is a parabola-shaped curve which contains the stable attractors and the singularity.

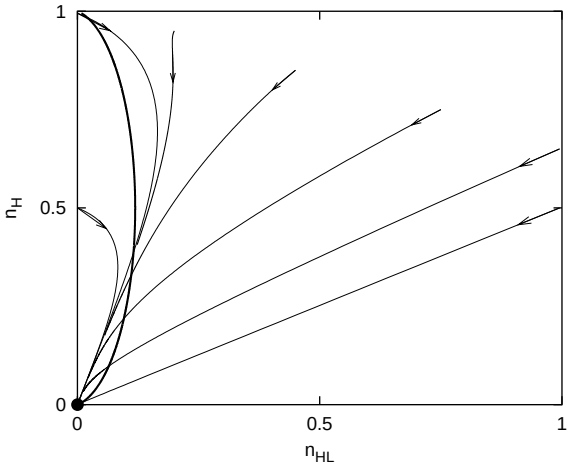

Fig. 4. Flow diagram of the kinetic Ising-like system, in the low-temperature (50 K), monostable conditions. All other parameter values are those of Figures 1 and 3. The trajectories have a single attractor, and do not join the local equilibrium curve (bold line).

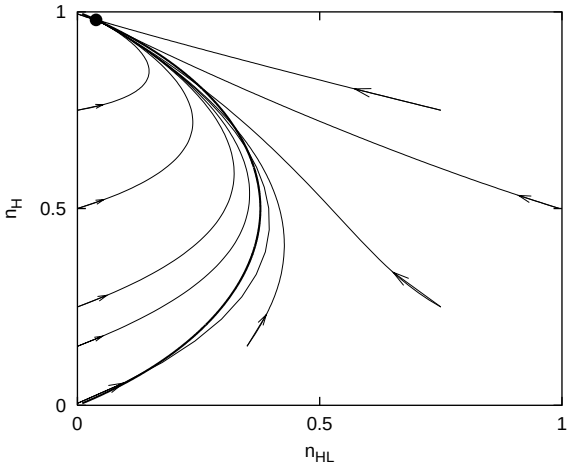

Fig. 5. Flow diagram of the kinetic Ising-like system, in the high-temperature (200 K), monostable conditions. All other parameter values are the same as in Figures 1, 3 and 4. The trajectories have a single attractor, and most of them approximatively join or follow the local equilibrium curve (bold line).

We have identified this parabola shaped curve to the "local equilibrium curve", resulting from the Huang approximation [21] which provides a one macroscopic parameter dynamic model. The local equilibrium approximation is obtained by constraining $n_{\mathrm{HL}}(t)$ to follow adiabatically $n_{\mathrm{H}}(t)$, *i.e.* $\frac{\mathrm{d}\overline{q}(t)}{\mathrm{d}t} = 0$ leading to the parabola equation, derived from equation (4.1) as:

$$n_{\mathrm{HL}} = \frac{-1 + \sqrt{1 + 4\left(1 - \mathrm{e}^{-K}\right) n_{\mathrm{H}}\left(1 - n_{\mathrm{H}}\right)}}{\left(1 - \mathrm{e}^{-K}\right)} \cdot \qquad (5.2)$$

We have plotted this "local equilibrium curve", computed for the parameter values of Figure 3, as a bold line. This curve is reminiscent of the "Most Probable Path" (MPP)

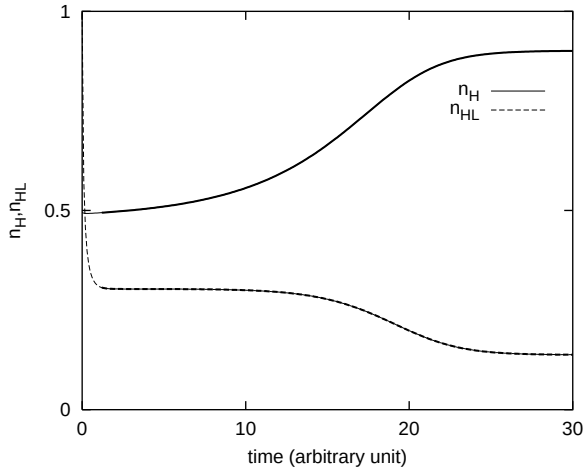

Fig. 6. Computed relaxation curves, $n_{\mathrm{H}}(t), n_{\mathrm{HL}}(t)$ in bistable conditions: all other parameter values are the same as in Figure 3. The successive relaxation regimes are illustrated: rapid onset of correlations reaching the local equilibrium, followed by a slow adiabatic evolution towards the long-range equilibrium state. These curves are associated with curve (a) of the flow diagram shown in Figure 3, with the bold part corresponding to the local equilibrium, *i.e.* to the pathway along the parabola. Arbitrary time scale means $E_{\mathrm{a}} = 0,\ \tau_0 = 1$.

described in a previous report [22] devoted to the study of the metastable states, following a novel macroscopic dynamics derived from the so-called "density-of-states sampling method" [23]. The Most Probable Path maximizes the probabilities along the relaxation path, and thus respects the local equilibrium conditions. A quantitative comparison between a local equilibrium curve and a MPP would not be obvious, however, since the latter is obtained in the frame of sampling methods, *i.e.* for finite size systems only.

It is worth emphasing the remarkable feature Figure 3 of trajectories occurring in two steps: (i) first, the system reaches the parabola, with a short range parameter (n_{HL}) which sizeably varies, while n_{H} remains almost constant, only adapting to the constraints equations (2.2–2.6); see Figures 6–8; (ii) then, the system reaches the nearest attractors, by following the parabolic path. The correlation and magnetization parameters simultaneously vary. The variations are much slower than during the first step. This step is reported as bold lines in Figures 6–8.

This observation in the bistable domain leads to distinguish two different timescales, one (short) for the short-order parameter and the other (long) for the variation of the long-range order parameter. From a physical point of view, it can be concluded that the evolution of the local probability density ($n_{\mathrm{HL}}(t)$) first reaches the local equilibrium and, later on, the long range parameter ($n_{\mathrm{H}}(t)$) evolves in order to reach the macroscopic equilibrium. This clears up the local equilibrium approximation used by Huang [21] which merely by-passes the former, rapid step in the relaxation path.

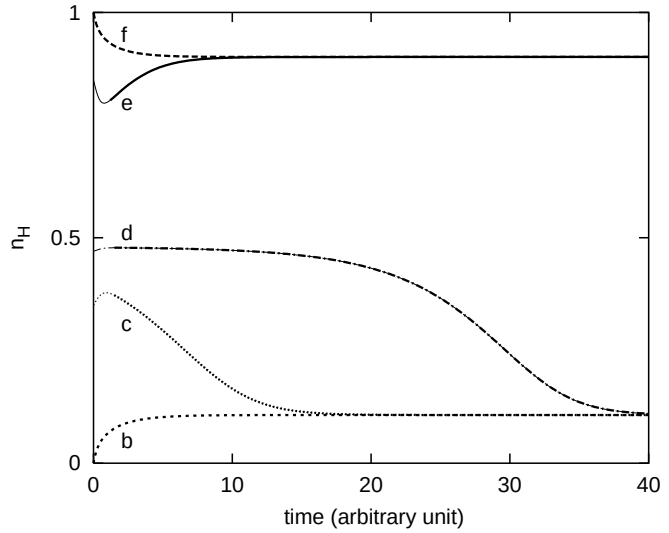

Fig. 7. Computed relaxation curves of the long-range order parameter $n_{\mathrm{H}}(t)$. Parameter values are those of Figure 6 (bistable conditions). Several typical initial states are considered: $n_{\mathrm{H}}(t=0) = 0,\ 0.35,\ 0.47,\ 0.85,\ 1$; for all of them we choose , $n_{\mathrm{HL}}(t=0) = 0$. Such a constraint on the short-range order parameter affects the transient regimes. The labels refer to the curves in (Fig. 3). The bold part of lines correspond to the local equilibrium, as in the previous figure.

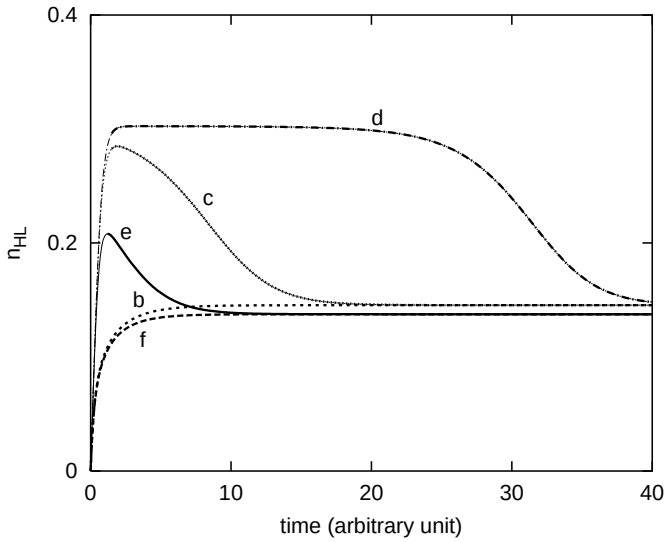

Fig. 8. Computed relaxation curves of the short-range order parameter $n_{\mathrm{HL}}(t)$, associated with the curves of Figure 7. From top to bottom (on the left side), initial values of $n_{\mathrm{H}}(t=0)$ were: 0, 0.35, 0.47, 0.85, 1. The labels refer to the curves of Figure 3, and bold part of lines correspond to the local equilibrium, as in the previous figures.

6 Low temperature relaxation curves: the effect of correlations

In this section we calculate the relaxation curves of the metastable state (HS fraction after LIESST), at different temperatures, in order to investigate the effect of correlations. The system is prepared, at low temperature, in the HS state ($n_{\mathrm{H}} = 1$, $n_{\mathrm{HL}} = 0$) and the relaxation is governed by the evolution equations. Due to the low-temperature situation, $\mathrm{e}^{-\beta(E_{\mathrm{a}}+\Delta)} \ll \mathrm{e}^{-\beta(E_{\mathrm{a}}-\Delta)}$, these equations write:

$$\frac{\mathrm{d}\overline{x}(t)}{\mathrm{d}t} = -\frac{2}{\tau_0}\mathrm{e}^{-\beta E_{\mathrm{a}}} C_+ \tag{6.1}$$

$$\frac{\mathrm{d}\overline{q}(t)}{\mathrm{d}t} = \frac{z}{\tau_0}\mathrm{e}^{-\beta E_{\mathrm{a}}} A_+ C_+. \tag{6.2}$$

For convenience these equations are re-expressed in terms of n_{H}, n_{HL}:

$$\frac{\mathrm{d}n_{\mathrm{H}}}{\mathrm{d}t} = -K_1 n_{\mathrm{H}} X\left(n_{\mathrm{H}}, n_{\mathrm{HL}}\right) \tag{6.3}$$

$$\frac{\mathrm{d}n_{\mathrm{HL}}}{\mathrm{d}t} = -K_2 n_{\mathrm{H}} Y\left(n_{\mathrm{H}}, n_{\mathrm{HL}}\right) \tag{6.4}$$

where:

$$K_1 = \frac{2}{\tau_0}\exp\left(-\beta\left(E_{\mathrm{a}} - \Delta + \frac{kT}{2}\ln\left(g\right)\right)\right) \tag{6.5}$$

$$K_2 = \frac{z}{2}K_1 \tag{6.6}$$

$$X\left(n_{\mathrm{H}}, n_{\mathrm{HL}}\right) = \left(\mathrm{e}^{-K} + \frac{n_{\mathrm{HL}}}{n_{\mathrm{H}}}\sinh\left(K\right)\right)^{z} \tag{6.7}$$

$$Y\left(n_{\mathrm{H}}, n_{\mathrm{HL}}\right) = \left(\mathrm{e}^{-K} + \frac{n_{\mathrm{HL}}}{n_{\mathrm{H}}}\sinh\left(K\right)\right)^{z-1} \times \left(\mathrm{e}^{-K} - \frac{n_{\mathrm{HL}}}{n_{\mathrm{H}}}\cosh\left(K\right)\right). \tag{6.8}$$

Due to the non-linear character of the functions X, Y, these equations have to be solved numerically by the modified midpoint routine. The results are reported in Figure 9, in which $n_{\mathrm{H}}(t)$ and $n_{\mathrm{HL}}(t)$ are plotted. It clearly appears that the relaxation curves have the expected sigmoidal shape (previously obtained in the mean-field approaches [3,4]) but, in addition, exhibit a noticeable slowing down at long times, as expected from the effect of correlations [9].

We have resolved the evolution equations (3.12, 3.13) using the local equilibrium (Huang [21]) approximation. In this approximation only the parabolic path of the flow diagram is followed (the initial state is defined by $n_{\mathrm{H}}(0)$ alone and also obeys the local equilibrium). The single, one-variable evolution equation gives $n_{\mathrm{H}}(t)$, as obtained by Huang in [21]. It is worth comparing the results on this one-variable approach to those of the two-variable model

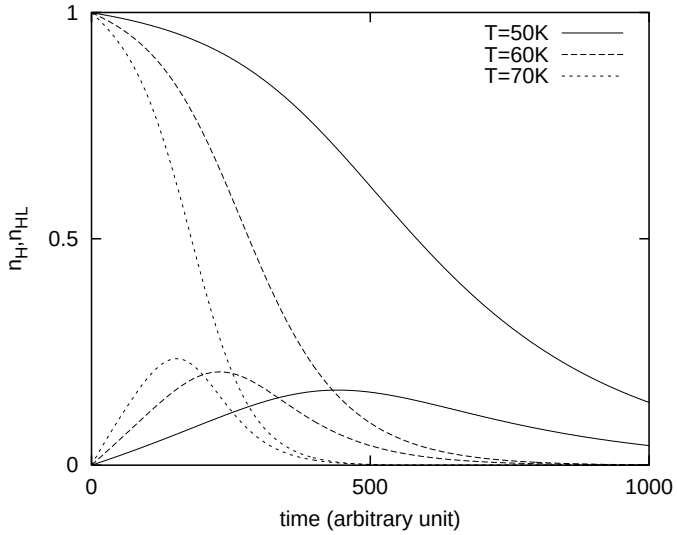

Fig. 9. Computed relaxation curves, $n_{\rm H}(t), n_{\rm HL}(t)$ at different temperatures (T = 50, 60 and 70 K). The initial sigmoidal shape of the curve and the consecutive slowing down due to the effect of correlations, are evidenced. On increasing the temperature, the relaxation time decreases. The parameter value are: J = 50 K, g = 150, Δ = 300 K, $E_{\rm a}$ = 400 K and τ_0 = 1 (arbitrary time unit).

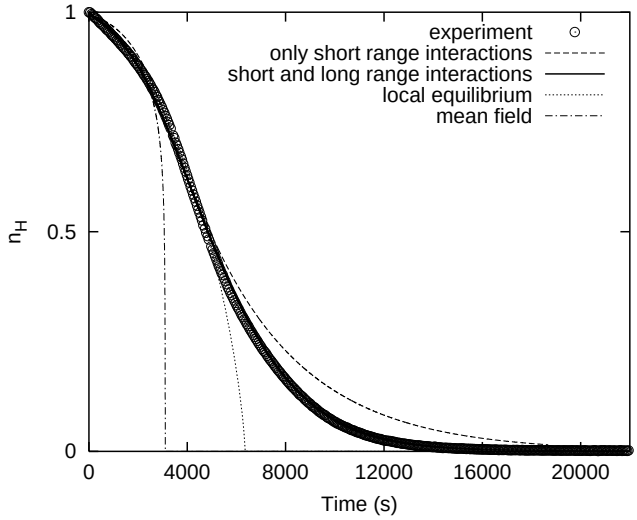

Fig. 10. Relaxation curve of the HS fraction of $[Fe_{0.52}Ni_{0.48}(btr)_2(NCS)_2] \cdot H_2O$ at T = 40 K. The best fitted curves (full line) perfectly matches to the experimental data (circles). It takes into account both long and short range interactions in the two macro-variable approach. Parameter values are: J = 52 K, J_l = 21 K, g = 3 000, Δ = 540 K, $E_{\rm a}$ = 835 K. The other curves have been computed with parameter values chosen so as to reproduce the width of the static hysteresis loop, but accounting for different constraints: mean field, local equilibrium, purely short range interaction (see corresponding labels in the figure).

developed in the present report. The following features have been observed:

– At low temperatures, where correlations are crucial because reaching the local equilibrium ($n_{\rm H} = 0$) requires very long times, the relaxation curves given by the 2- and 1-variable treatments are very different, namely the time dependences of the correlations, $n_{\rm HL}\,(t)$, are qualitatively different, and the relaxation tails are not provided by the 1-variable treatements (see Fig. 10). Precisely, the maximum of $n_{\rm HL}\,(t)$, in the 1-variable treatment, occurs at $n_{\rm H} = 0.5$, and this characterizes a $n_{\rm HL}$ dynamics which strictly follows that of $n_{\rm H}$. In the 2-variable treatment (see Fig. 9), $n_{\rm HL}\,(t)$ reaches a maximum at a time t such that $n_{\rm H} > 0.5$. These differences can be illustrated in the flow diagrams. The point is that the trajectories reach the parabola only around $n_{\rm H} \simeq 1$.
– At higher temperatures, the correlations are not so crucial, and the local equilibrium method can be considered as a good approximation for the time dependence of the long-range order parameter.

7 Comparison to experimental data

We have performed photoexcitation (LIESST) using a 550 nm wavelength on the Fe^{II} spin-crossover solids $[Fe_pNi_{1-p}(btr)_2(NCS)_2] \cdot H_2O$, and present data for the selected composition $p = 0.52$. Relaxation in the dark was followed by a SQUID magnetometer (see [24,25] for experimental details). Only selected data are presented here, for the purpose of the discussion of the present model.

After photoexcitation, the system is considered to be entirely populated in the HS state. The initial state is thus defined by $n_{\rm H} = 1$ and $n_{\rm HL} = 0$. Of course, the actual initial state is not so perfect, with a slightly incomplete (and inhomogenous) excitation state. A distribution of initial populations might be straightforwardly introduced, but is not crucial for controlling the relevance of the model. Also, the investigation of diluted systems only aims to provide systems with the desired degree of cooperativity. The basic study of the interactions (nature, range, evolution with the degree of dilution) is not addressed here. We merely treat the diluted system in a uniform approximation.

The results of the two variable-model and its one-variable approach are also compared to those of the mean-field approximation, which are governed by the following equation:

$$\frac{{\rm d}n_{\rm H}}{{\rm d}t} = -Kn_{\rm H}{\rm e}^{-\alpha n_{\rm H}} \qquad (7.1)$$

where $\alpha = 2\beta zJ$.

A typical result is shown in Figure 10. We have observed that, the more cooperative the system, the worse is the agreement with the mean-field approximation, mostly at long time. Then correlations cannot be neglected. However, for short times, and weakly cooperative systems, the mean-field and the present 2-variable dynamics are both in good agreement with the experiments. We have evidenced, in the Section 5, two time scales, a short one, associated with the onset of the local equilibrium, and a long one, respectively associated with the simultaneous evolutions of the short-range and long-range order parameters. Now, the picture of the relaxation

of the system appears more subtle; precisely, the effect of correlations is crucial at all time scales, at short times for the (more or less) rapid convergence towards the local equilibrium, and at long times, when the development of correlations is responsible for the "extra" slowing down of the relaxation rate.

We have improved the agreement between the 2-variable model and the experimental curves, see Figure 10, by introducing long-range interactions which reduce the amplitude of the tail effect. Indeed, it is now admitted [18,26] that both interactions should be present in spin-crossover solids, and the tail effect enables us to weight the short- and long-range interactions. Thus the relaxation curves should provide a novel access to the investigation of interactions [27]. Indeed, the usual strategy based on dilution faces serious difficulties (see for instance [28]), due to the large number of parameters involved: ligand-field, degeneracies in addition to the specific interaction parameters, all of them presumably being sizeably dependent on the dilution state of the solid, through structural effects.

8 Conclusion

In this work, we have investigated the effect of correlations on the relaxation curves of the HS fraction in spin-crossover systems. For this, we have adapted the macroscopic dynamics introduced in the 70's by par Kubo *et al.*, to the Ising-like Hamiltonian. We have introduced the correlations according to the Bethe-Peierls method, and obtained a set of coupled evolution equations for the two macrovariables: magnetization and first-neighbour correlations. An excellent agreement with the experimental curves has been obtained, including the so-called "tail-effect" which consists in an extra slowing-down of the relaxation for strongly cooperative systems at long times. We thus confirmed that the tail effect is associated with the onset of correlations. This result is promising for the investigation of interactions in spin-crossover solids, which till now are not fully understood. Another access to the ratio short *vs.* long range interaction also emerges from the analysis of the percolation threshold of the dilute system.

For a better understanding of the dynamics of the two macrovariable model, we have determined the flow diagrams in the parameter space of the system. We found, in the bistable case of the static system, a relaxation made of two stages, an initial (and shorter) stage leading to the local equilibrium dynamics involved in the Huang approximation. During this stage the short-range parameter adiabatically follows the long-range parameter. The trajectories rapidly join the local equilibrium curve. During the second stage, both parameters slowly evolve together, obeying the local equilibrium.

At low temperature, the two time scales are no longer distinct, and the local equilibrium is not longer reached. Indeed, the flow diagram trajectories are quite far from the local equilibrium curve. Accordingly, the relaxation curves computed according to the local equilibrium approach qualitatively differ from those of the present 2-variable model. The latter, in turn, perfectly reproduce the available experimental data.

We acknowledge J. Haasnoot for providing us the samples, A. Hauser for useful discussion and J. Hodges for a critical reading of the manuscript. LMOV is supported by CNRS as "Unité Mixte de Recherche" (UMR 8634). The CEE financial support (TMR action TOSS, contract CT98-0199) is acknowledged.

References

1. P. Gütlich, Struct. Bonding (Berlin) **44**, 83 (1981); E. König, Struct. Bonding (Berlin) **76**, 51 (1991); O. Kahn, Cur. Op. Solid State Mater. Sci. **1**, 547 (1996).
2. S. Decurtins, P. Gütlich, C.P. Köhler, H. Spiering, A. Hauser, Chem. Phys. Lett. **1**, 139 (1984); P. Gütlich, A. Hauser, H. Spiering, Angew. Chem. Int. Ed. Engl. **33**, 2024 (1994); A. Hauser, Comments Inorg. Chem. **17**, 17 (1995).
3. A. Hauser, Coord. Chem. Rev. **11**, 275 (1991); A. Hauser, P. Gütlich, H. Spiering, Inorg. Chem. **25**, 4345 (1986); A. Hauser, J. Chem. Phys. **94**, 2741 (1991).
4. K. Boukheddaden, I. Shteto, B. Hoo, F. Varret, Phys. Rev. B (in press).
5. J. Wajnflasz, R. Pick, J. Phys. Colloq. France **32**, C1 (1971).
6. A. Bousseksou, J. Nasser, J. Linares, K. Boukheddaden, F. Varret, J. Phys. I France **2**, 1381 (1992).
7. A. Bousseksou, F. Varret, J. Nasser, J. Phys. I France **3**, 1463 (1993).
8. S. Doniach, J. Chem. Phys. **68**, 4912 (1978).
9. H. Romstedt, H. Spiering, P. Gütlich, J. Phys. Chem. Solids **59**, 1353 (1998).
10. Y. Saito, R. Kubo, J. Stat. Phys. **15**, 223 (1976).
11. M. Suzuki, R. Kubo, J. Phys Soc. Jap. **24**, 51 (1968).
12. H.A. Bethe, Phys. Rev. **54**, 995 (1938).
13. N.G. van Kampen, Can. J. Phys. **39**, 551 (1961).
14. N.G. van Kampen, in *Stochastic Processes in Physics and Chemistry* (North Holland, Amsterdam, 1981).
15. Y. Takagi, J. Phys. Soc. Jpn **4**, 99 (1949).
16. R.J. Glauber, J. Math. Phys. **4**, 294 (1963).
17. *Numerical Recipes* (Cambridge University Press, 1992).
18. J. Linares, H. Spiering, F. Varret, Eur. Phys. J. B **10**, 271 (1999).
19. R.H. Fowler, E.A. Guggenheim, *Statistical Thermodynamics* (Cambridge University Press, London, 1939).
20. J.P. Martin, J. Zarembowitch, A. Dworkin, J. Haasnoot, E. Codjovi, Inorg. Chem. **33**, 2617 (1994).
21. H.W. Huang, Phys. Lett. A **48**, 395 (1974).
22. I. Ishteto, J. Linares, F. Varret, Phys. Rev. E **56**, 5128 (1997).
23. J. Lee, M.A. Novotny, P.A. Rikvold, Phys. Rev. E **52**, 356 (1995).
24. A. Desaix, O. Roubeau, J. Jeftic, J.G. Haasnoot, K. Boukheddaden, E. Codjovi, J. Linares, M. Nogues, F. Varret, Eur. Phys. J. B **6**, 183 (1998).
25. H. Constant Machado, Ph.D thesis, Orsay (1997).
26. N. Willenbacher, H. Spiering, J. Phys. C. **21**, 1423 (1988); H. Spiering, N. Willenbacher, J. Phys. Cond. Matter. **1**, 10089 (1989).
27. K. Boukheddaden, J. Linares, H. Spiering, F. Varret, Eur. Phys. J. B **15**, 317 (2000).
28. H. Constant, J. Linares, F. Varret, J. Hassnoot, J.P. Martin, J. Zarembowitch, A. Dworkin, A. Bousseksou, J. Phys. I France **6**, 1203 (1996).